ECS Journal of Solid State Science and Technology, **4** (9) N117-N123 (2015)
2162-8769/2015/4(9)/N117/7/$33.00 © The Electrochemical Society

Observation of Water-Droplet Impacts with Velocities of O(10 m/s) and Subsequent Flow Field

Y. Tatekura,[a] T. Fujikawa,[a] Y. Jinbo,[a] T. Sanada,[b,*] K. Kobayashi,[a] and M. Watanabe[a,z]

[a]*Division of Space and Mechanical Engineering, Hokkaido University, Sapporo, Hokkaido 060-8628, Japan*
[b]*Department of Mechanical Engineering, Shizuoka University, Hamamatsu, Shizuoka 432-8561, Japan*

A two-fluid spray cleaning technique has been gaining popularity as a cleaning process in the semiconductor industry. The most essential physical process in this technique is the impact of droplets with a velocity of O(10 m/s) on a solid surface. This study aims to experimentally and numerically investigate water-droplet impacts with velocities of up to 50 m/s and their subsequent flow fields, especially the gas flow field in the strictly limited area in the vicinity of the contact line. First, we experimentally evaluated the velocity of the splash and numerically calculated the gas velocities. Comparison of these velocities supported our assumption that the maximum gas velocity may be on approximately the same order as the velocity of the splash. Therefore, we concluded that the gas velocity field of the order of 500 m/s indeed develops at the impact of droplet with a velocity of the order of 50 m/s. Moreover, we determined that the gas pressure was of the order of 1.0 MPa by numerical analysis. Such a high pressure leads to shock wave propagation, which can contribute to the cleaning process in semiconductor production.

Manuscript submitted June 23, 2015; revised manuscript received July 21, 2015. Published August 11, 2015. This was Paper 2038 presented at the Boston, Massachusetts, Meeting of the Society, October 9-14, 2011.

To manufacture semiconductors, cleaning techniques that use physical action, such as megasonic agitation, are generally employed[1] together with those using chemical action to enhance the cleaning efficiency. A deionized water/gas-mixture jet spray cleaning technique, in other words, a two-fluid spray cleaning technique, is also gaining popularity.[1–4] The advantage of this technique over megasonic agitation is the magnitude of the physical action generated by a high-speed droplet impacting a solid surface. However, most cleaning techniques that use physical action tend to cause structural damage and pattern collapse; therefore, the particle removal force should be quantitatively understood and measured.[5,6] The development of advanced spray technology offers the possibility of preventing this damage by controlling both the sizes and velocities of the droplets with extremely high accuracy.[7,8]

It should be emphasized here that the most essential physical process in this two-fluid spray cleaning technique is the droplet impact upon the solid surface with a velocity of several tens of meters per second. Until recently, the velocities of liquid droplets in most experimental studies on liquid-droplet impacts were restricted to the range of several meters per second,[9–11] mainly due to the difficulties associated with high-speed observation. On the other hand, Mehdizadeh et al.,[12] Pan et al.,[13] and Visser et al.[14] reported on experimental studies that utilized droplet impacts at velocities of the order of 10 m/s. Mehdizadeh et al.[12] observed the impacts of water droplets with radii of about 1 mm on stainless steel surface mounted on the end of a rotating arm whose linear velocities of up to 50 m/s. They measured the number of fingers and maximum diameter of the droplet after spreading. Pan et al.[13] observed the collision between a solid plate and a droplet with a radius of about 0.5 mm and a speed of 42 m/s, which was initially driven by upstream air flow through a nozzle and accelerated to nearly the same velocity as that of the high-speed flow downstream. They investigated the various splashing mechanisms and the expanding lamella. Visser et al.[14] produced a train of monodisperse droplets by forcing Rayleigh break-up of the liquid jet and then deflected a droplet from the train by applying an electrical pulse, resulting in the impact of a single droplet with a radius of about 50 μm on an impact plate at a velocity of up to 50 m/s. They investigated the spreading dynamics, maximal spreading diameter, boundary layer thickness, and rim formation. However, in all of these studies, attention was focused exclusively on the investigation of the contribution of the liquid flow to the droplet impact.

Xu et al.,[15] on the contrary, focused their attention on the investigation of the contribution of the gas flow to the droplet impact. They demonstrated that the presence of a surrounding gas is essential for splashing to occur on a dry flat surface. Inspired by their findings, computational investigations of the gas flow following a droplet impact on a solid surface have been conducted;[16,17] however, these investigations were restricted to incompressible fluid flow analysis. Bang et al.[17] investigated splashing mechanisms using the boundary element method for incompressible fluids to account for the effect of gas pressure explored by Xu et al. at moderate impact velocities. Their computations showed that the air velocity exceeded the impact velocity of the droplet by more than a factor of 3.

We, in turn, were inspired by their results, realizing that the gas flow velocities that developed after the droplet impacts in their studies could reach considerably high values when the impact velocity was 50 m/s. Hence, it was evident that compressible fluid flow analysis was urgently required to study the gas flow developed after the droplet impact, since gas compressibility plays a dominant role in the development of gas flow fields with high velocities. We also recognized that the pressure of the gas flow could play an important role in cleaning techniques, since a substantial velocity may correlate with a substantial pressure, i.e., a shock wave. It should be recalled that in the laser shock cleaning (LSC) method[6] there is a strong correlation between the removal of a particle and the dynamics of the laser-induced shock wave.

We investigate water-droplet impacts with velocities of up to 50 m/s and the subsequent velocity fields, especially focusing on experimental and numerical analysis of the gas velocity fields. We also investigate the pressure fields that developed after the droplet impact. First, the velocity of the splash, which was considered to be a gas-liquid, two-phase mist flow, was evaluated by processing images taken by high-speed photography at rates of up to one million frames per second; then, both the velocity and pressure fields of the gas flow that developed after the droplet impacts were numerically evaluated by solving the Euler equation[18,19] for a two-phase compressible fluid by using the third-order TVD Runge–Kutta scheme, third-order ENO-LLF scheme,[20] and hybrid particle level set method.[21] Compressible flow analysis is critical in the investigation of high-speed gas flows. In this paper, we will also discuss whether the gas pressure fields that developed after droplet impacts could contribute to the cleaning process by examining the shock wave dynamics in the LSC method.

Experimental and Numerical Methods

Both experimental and numerical analyses were used to investigate water-droplet impacts with velocities of up to 50 m/s and the subsequent velocity fields, focusing on that of the gas, and ex-

*Electrochemical Society Active Member.
zE-mail: masao.watanabe@eng.hokudai.ac.jp

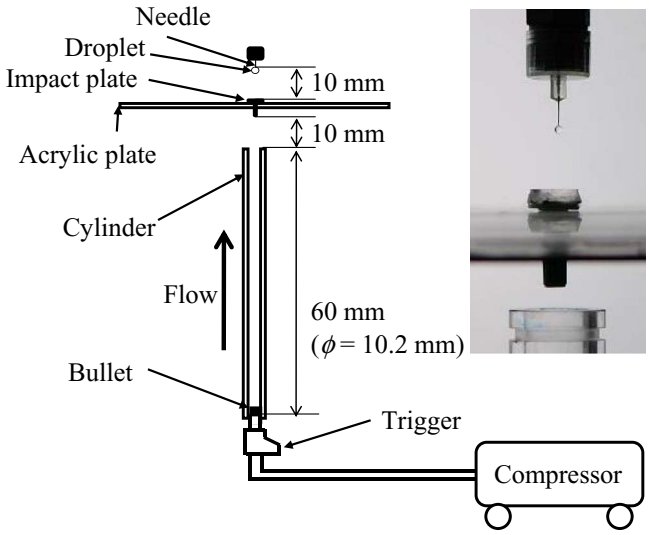

Figure 1. Experimental setup for high-speed droplet impacts with velocity of O(10 m/s). Bullet set at lower end of acrylic cylinder tube was accelerated by compressed air at pressures ranging from 0.05 MPa to 0.60 MPa in gauge.

amined whether gas flow could contribute to the cleaning process used in semiconductor manufacturing. We performed two types of experiments: free-fall droplet-impact experiments and investigations of droplet impacts on an accelerated solid plate. These two experiments are considered to be equivalent in a Galilean transformation regarding the droplet motion; however, no Galilean transformation of the gas flow field holds in these experiments. Hence, the influence of the gas flow on the development of the subsequent flow field after droplet impact was investigated by comparing these two experimental results.

We observed a single liquid water droplet freely falling onto a solid plate made of a transparent acrylic resin by using a high-speed video camera (Shimadzu Corporation, HyperVision HPV-1). A single liquid-water-droplet with diameters of approximately 2 mm, was generated on the end of a needle with inner and outer diameters of 0.1 mm and 0.25 mm, respectively. After a period of time, the droplet was pinched off from the nozzle due to gravity. The impact velocities of the droplets on the surface, which were controlled by varying the height of the needle above the solid surface from 100 mm to 600 mm, were measured from the pictures taken by the high-speed video camera.

We also observed a suspended stationary single liquid-water-droplet impact on an accelerated solid plate, which we refer to as an impact plate hereafter, by using the high-speed video camera. Figure 1 shows a schematic of the experimental setup; a single liquid-water-droplet was generated with the same needle that was used in the freefall experiment. The diameter of the droplet was approximately 2 mm, and the generated droplet was suspended on the end of the needle. The circular impact plate with an outer diameter of 8.0 mm and a height of 1.0 mm was made of transparent acrylic resin. This impact plate was adhered to a T-shaped launch mount, as shown in Figure 2a. The distance between the initial position of the impact plate and the lower edge of the suspended droplet was set to 10 mm.

A bullet, which is shown in Figure 2b, was set at the bottom of an acrylic cylinder tube with an inner diameter of 10.2 mm and a height of 60 mm, as shown in Figure 1. As the electric valve set at the outlet of a compressor was opened, the bullet was accelerated by compressed air at a gauge pressure between 0.05 MPa and 0.60 MPa and collided with the bottom of the impact plate; thus, the impact plate was projected up toward the suspended droplet. The rates of change of both the droplet shape and liquid droplet flow field upon impact were measured from the pictures taken by the high-speed video camera. This camera can be used at frame rates between 100,000 fps and 525,000 fps. A strobe

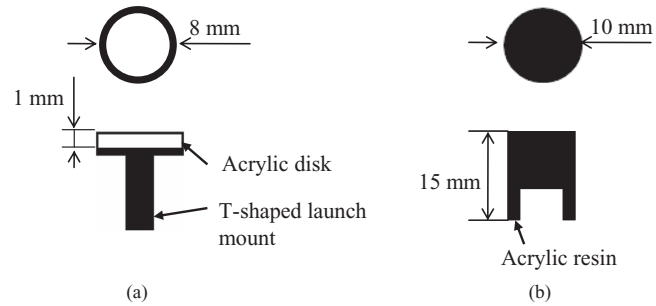

Figure 2. Schematic of the (a) impact plate and (b) bullet. Circular impact plate made of transparent acrylic resin was adhered to T-shaped launch mount.

scope (SA-200F) by Nissin Electronic Co. Ltd. was used as the back light source.

We numerically solved the Euler equation[18,19] for a two-phase compressible fluid in an axisymmetric two-dimensional coordinate system:

$$\frac{\partial \boldsymbol{Q}}{\partial t} + \frac{\partial \boldsymbol{F}}{\partial r} + \frac{\partial \boldsymbol{G}}{\partial z} = \boldsymbol{S}, \quad [1]$$

where

$$\boldsymbol{Q} = \begin{pmatrix} \rho \\ \rho u_r \\ \rho u_z \\ E \end{pmatrix}, \ \boldsymbol{F} = \begin{pmatrix} \rho u_r \\ \rho u_r^2 + p \\ \rho u_r u_z \\ (E+p)\, u_r \end{pmatrix}, \ \boldsymbol{G} = \begin{pmatrix} \rho u_z \\ \rho u_r u_z \\ \rho u_z^2 + p \\ (E+p)\, u_z \end{pmatrix},$$

$$\boldsymbol{S} = -\frac{1}{r} \begin{pmatrix} \rho u_r \\ \rho u_r^2 \\ \rho u_r u_z \\ (E+p)\, u_r \end{pmatrix}, \quad [2]$$

where ρ is the density, p is the pressure, and u_r and u_z are the flow velocity components in the r and z directions, respectively. E is the total energy, which is expressed as

$$E = \rho e + 0.5\rho \left(u_r^2 + u_z^2\right), \quad [3]$$

where e is the internal energy per unit mass.

In this study, we used air for the gas and water for the liquid. In order to close the Euler equations, we employed the following stiffened equation of state:[22]

$$p = (\gamma - 1)\, \rho e - \gamma \Pi, \quad [4]$$

where γ and Π are constants ($\gamma = 1.4$ and $\Pi = 0$ Pa for air, and $\gamma = 4.4$ and $\Pi = 6 \times 10^8$ Pa for water). The third-order TVD Runge–Kutta scheme[20] was employed to evolve the equations forward in time. Furthermore, the third-order ENO-LLF scheme[20] was used to calculate the convection term.

The level set method[23] was employed to locate the gas-liquid interface. The equation that governs the advance of the level set function, ϕ, can be expressed as

$$\frac{\partial \phi}{\partial t} + u_r \frac{\partial \phi}{\partial r} + u_z \frac{\partial \phi}{\partial z} = 0. \quad [5]$$

The level set function is usually the signed distance function with re-initialization to maintain accuracy. In the present study, Eq. 5 was numerically solved by the third-order TVD Runge–Kutta scheme and fifth-order WENO scheme.[24] Additionally, the hybrid particle level set method[21] was used to improve the mass conservation properties of the level set method.

The ghost fluid method[25] was used to eliminate the dispersion and dissipation errors. This method defines ghost cells in the neighborhood of the interface in the calculation domain. Thus, two fluids were present in this analysis: the real fluid and the ghost fluid. It was sufficient to define the ghost fluid values only in the vicinity of the interface. The ghost fluid of the liquid was defined by using one-sided extrapolation of the entropy and velocities to the other side of

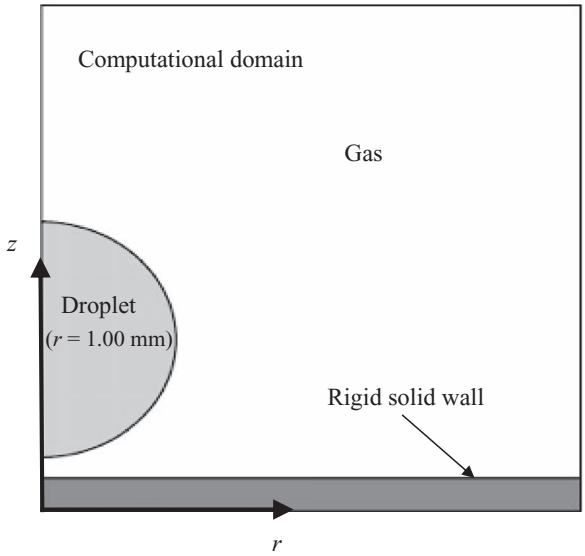

Figure 3. Schematic of the computational domain. The center of a droplet with 1.00 mm radius was initially set 1.04 mm above rigid solid wall surface in calculation domain with dimensions of 4.00 mm × 4.00 mm.

the interface, and the pressure of the ghost fluid was set equal to that of the real fluid (gas). The ghost fluid of the gas was defined by extrapolating the entropy, pressure, and tangential velocity. The normal velocity of the ghost fluid was set equal to that of the liquid.

The computational domain is shown in Figure 3. The center of a droplet with a radius of 1.00 mm was initially set 1.5 mm above the surface of a rigid solid wall in a calculation domain with dimensions of 14 mm (perpendicular to the wall) × 16 mm (parallel to the wall). The initial velocities of both the gas and liquid phases were uniform, the initial pressures of both phases were 0.10 MPa, and the densities of the gas and liquid phases were 1.20 kg/m^3 and 1000 kg/m^3, respectively. Adaptive zonal grids[26] were applied in the computation. The finest grid resolution and smallest time increment were 0.0025 mm and 5.0 × 10^{-10} s, respectively.

Results and Discussion

We measured the impact plate velocities, U_{ip}, in the range of compressed-air pressures from 0.05 MPa to 0.60 MPa in gauge. Figure 4 shows the results. We evaluated U_{ip} by arithmetically averaging

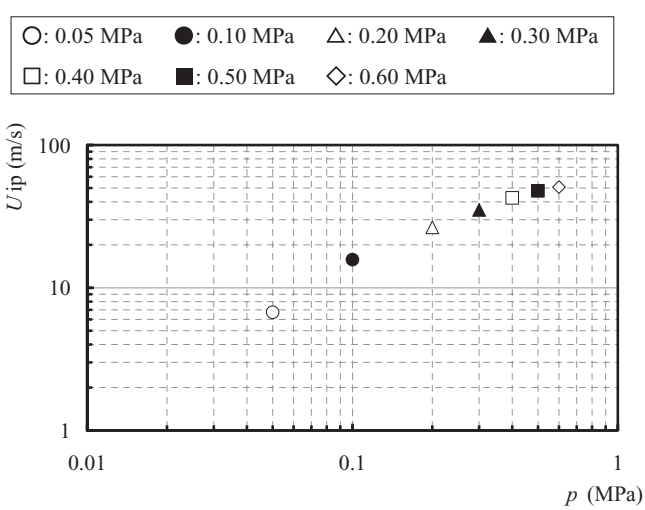

Figure 4. Velocity of impact plate, U_{ip}, at compressed air pressures from 0.05 MPa to 0.60 MPa in gauge. Impact plate velocities are approximately between 2 m/s and 50 m/s.

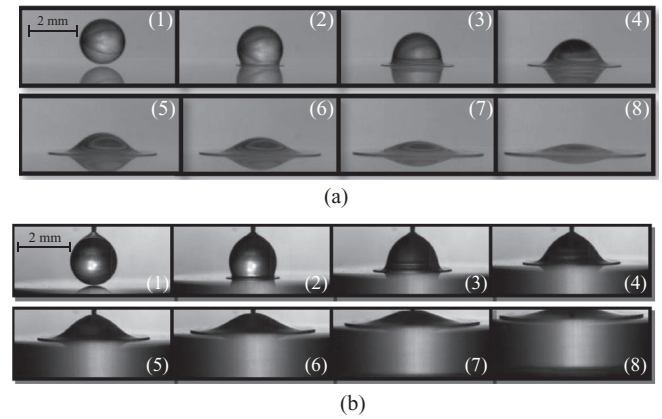

Figure 5. Deformation of single droplet on solid surface immediately after impact: low-impact velocity cases. (a) Freely falling single droplet with impact droplet velocity, U_D, of 3.0 m/s with time step of $\Delta t = 100$ µs. (b) Impact plate impacting suspended single droplet with impact plate velocity, U_{ip}, of 3.0 m/s and time step of $\Delta t = 100$ µs.

three measurements taken under the same experimental conditions. The impact plate velocities were found to be approximately in the range from 2 m/s to 50 m/s; hence, the impact plate velocity could be controlled by adjusting the compressed-air pressure from a relatively low velocity (such as the droplet free-fall velocity) to a relatively high velocity, so that the splash could be observed upon impact, as will be discussed later.

First, we discuss the low-velocity cases. The deformation of a single droplet impacting on the solid surface was observed as a function of time. Figure 5a shows the results for the free-fall of a single droplet with an impact droplet velocity, U_D, of 3.0 m/s, and Figure 5b shows the results obtained by impacting a plate on a single suspended droplet at a velocity, U_{ip}, of 3.0 m/s. An axisymmetric liquid film that flowed radially outward was observed (Figure 6). We could evaluate the radial velocity, U_R, of this liquid film by measuring the velocity of its rim, that is, the contact line velocity.

We compare U_R of the contact line obtained from the free-fall and impact-plate experiments. Figure 7 shows the U_R of the contact line in the left direction, measured at various nondimensionalized radial distances, r_R/r_D, where r_R is the distance from the axis and r_D is the droplet radius just before impact. The radial velocity of the contact line obtained from the free-fall experiments agrees well with that obtained from the impact-plate experiments. No significant differences are observed between the results obtained from the free-fall and impact-plate experiments in terms of the droplets' deformation rates upon impact; therefore, we conclude that the influence of the gas flow on the development of the subsequent liquid flow field after droplet impact is insignificant in the low-velocity cases.

Next, we examine the high-velocity cases. Figures 8a and 8b show the droplet deformation on the impact plate when the plate impacted the droplet at higher velocities: $U_{ip} = 22.0$ m/s and $U_{ip} = 53.0$ m/s, respectively. The droplet shapes after the impacts at high velocities are significantly different from those at low velocities. Figure 9 shows a close-up of Figure 8b(2). The area indicated by arrow (a) is darker than

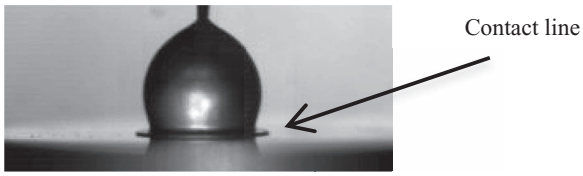

Figure 6. Snapshot of axisymmetric liquid film flowing radially outward. Liquid film radial velocity, U_R, was calculated by measuring velocity of liquid film edge, i.e., velocity of contact line indicated by arrow.

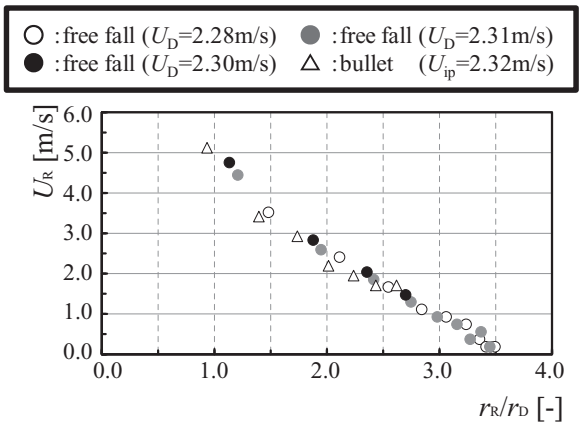

Figure 7. Comparison of radial velocities, U_R, of contact line obtained from free-fall and impact-plate experiments at various nondimensionalized radial distances r_R/r_D, where r_R is distance from axis and r_D is droplet radius just before impact. Contact line radial velocity obtained from free-fall and impact-plate experiments agrees well.

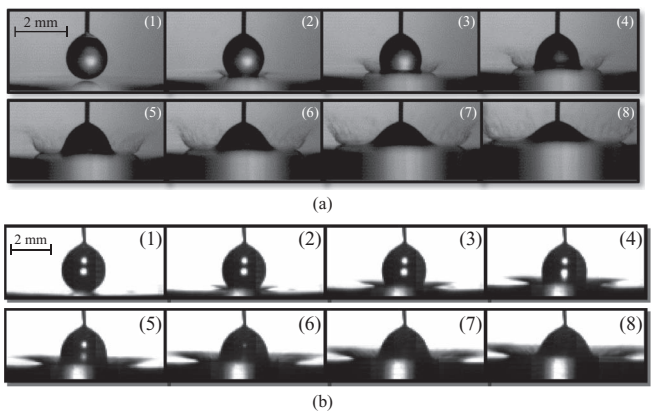

Figure 8. Deformation of a single droplet on solid surface immediately after impact: high-impact velocity cases. (a) Impact plate impacting suspended single droplet with velocity, U_{ip}, of 22.0 m/s and time step of $\Delta t = 7.6$ µs and (b) with impact plate velocity, U_{ip}, of 53.0 m/s and time step of $\Delta t = 1.9$ µs. A splash is observed.

the surrounding areas, suggesting the existence of a liquid. However, this area is notably brighter than the areas that are known to be filled with liquid, thereby excluding the possibility of a single-phase pure liquid. We consider that the arrow (a) points to the tip of a splash that consists of numerous minute droplets. The r-direction velocity of the splash, U_s, was calculated by tracking the position of the tip in the sequential images.

Figure 10 shows U_s measured with various values of U_{ip}. The uncertainties of U_s, which were mainly introduced in the determination of the tip location based on sequential images with an extremely high frame rate, are typically 4.8 m/s and 50 m/s for $O(U_s = 10$ m/s) and $O(U_s = 100$ m/s), respectively.

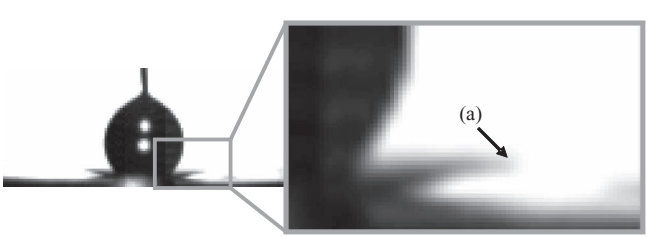

Figure 9. Snapshot of splash development.

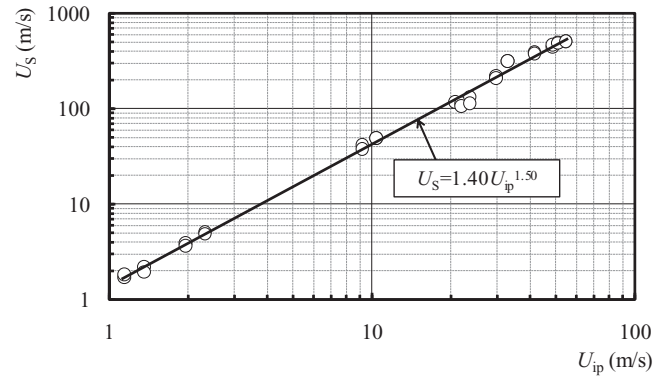

Figure 10. r-direction splash velocity, U_S, measured approximately 1 mm from droplet central axis. This velocity can be well correlated with impact velocity: $U_S = 1.40U_{ip}{}^{1.50}$. For lower velocities ($U_{ip} < 2.4$ m/s), U_R was substituted for U_S because no splash was observed.

For lower velocities ($U_{ip} < 2.4$ m/s), U_s was substituted into U_R. These velocities can be well correlated with the impact velocity as follows:

$$U_s = 1.40U_{ip}{}^{1.50}, \qquad [6]$$

where U_s is approximately 500 m/s when $U_{ip} = 50$ m/s. Since a splash can be accelerated by a surrounding gas, the maximum gas velocity may be on approximately the same order as U_s. This result suggests that a gas flow field with a substantial velocity can develop following droplet impact. We then numerically analyzed the gas flow field.

Figure 11 shows the distributions of the magnitude of the r-direction gas velocity in the rectangular area in Figure 12 that were numerically calculated. The initial radius of the droplet, r_D, was 1.0 mm, and the initial position of the center of the droplet was 1.5 mm from the solid surface. Both the liquid and gas were initially at rest. At time $t = 0$ s, z-direction velocities of -50 m/s were applied to both the gas and the liquid. The resulting r-direction gas velocity was of the order of 500 m/s at $t = 10.21$ µs in the vicinity of $r = 0.18\ r_D$.

Figure 13 shows both the r-direction velocity of the splash, U_s (which is correlated with the experimental results via Eq. 6), and the maximum value, U_g, of the numerically calculated r-direction gas velocities. A comparison of the velocities, U_s and U_g, supports our assumption that the maximum gas velocity may be on approximately the same order as U_s; hence, we can conclude that a gas velocity field of the order of 500 m/s indeed develops following a droplet impact at a velocity of the order of 50 m/s. The splash could not be observed in the numerical results because of the insufficient spatial resolution of the calculations. It is expected that splash observation would be possible even in the numerical results if the three dimensional calculations were performed with sufficient spatial resolution.

In this investigation, we could experimentally measure the gas velocity by utilizing the splash. On the other hand, Visser et al.,[14] who performed their own experiments under conditions equivalent to those of the spray cleaning used for semiconductors, did not observe the splash. Visser et al. experimentally investigated the impacts of droplets with diameters of the order of 10 µm and velocities of up to 50 m/s upon a surface.

The splash/non-splash boundaries of droplet impacts on dry surfaces have been studied.[27–30] They are most commonly described by the nondimensional numbers Re, We, and Oh, which are given by

$$\mathrm{Re} = \frac{2\rho r_D U_i}{\mu}, \ \mathrm{We} = \frac{2\rho r_D U_i^2}{\sigma}, \ \mathrm{Oh} = \frac{\sqrt{\mathrm{We}}}{\mathrm{Re}}, \qquad [7]$$

where ρ is the liquid density, r_D is the initial droplet radius, U_i is the impact velocity, μ is the liquid viscosity, and σ is the surface tension. Cossali et al.[29] proposed that splash can be observed when the following condition is satisfied:

$$\mathrm{Oh} \times \mathrm{Re}^{1.25} > 119.23. \qquad [8]$$

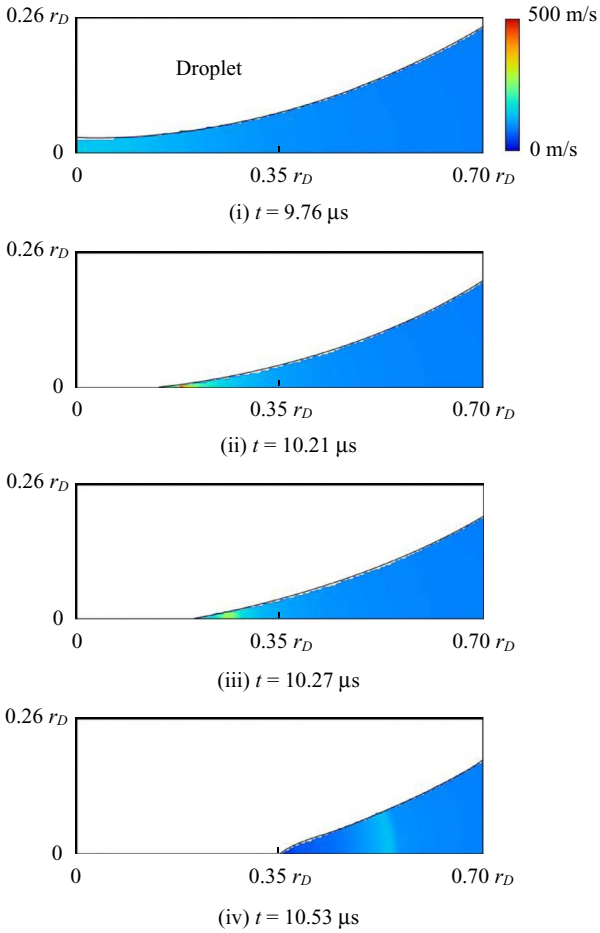

Figure 11. Numerically calculated distributions of r-direction gas velocity magnitudes in area shown in Figure 12. r-direction gas velocity is of the order of 500 m/s at $t = 10.21$ μs in the vicinity of $r = 0.18\ r_D$.

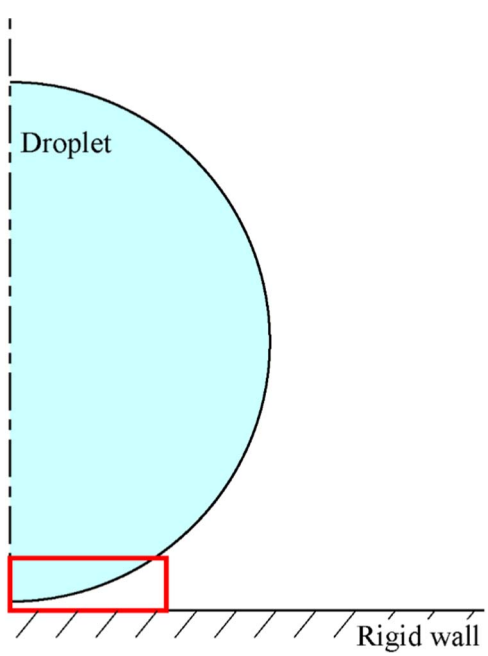

Figure 12. Area (small rectangle) where velocity field is drawn in Figure 11.

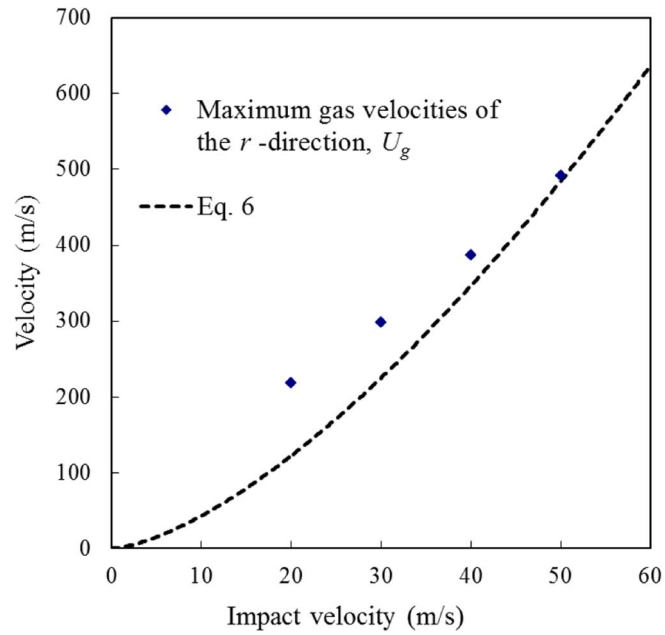

Figure 13. Maximum value of numerically calculated r-direction gas velocities, U_g, compared with experimentally obtained r-direction velocity of the splash, U_s. U_g is approximately equal to or greater than U_s.

The typical Oh × Re$^{1.25}$ values of Visser et al. and the present study are 87.5 and 4.09 × 10^3, respectively. This result indicates that our study may not be equivalent to investigation of the spray cleaning used in semiconductor processes in terms of the liquid flow development after droplet impact; however, it should be emphasized that studies that utilize these three nondimensional numbers neglect the gas flow that develops after liquid droplet impact.

Not only liquid flow but also gas flow plays a significant role in the flow field development after liquid droplet impact, as revealed by Xu et al.[15] They showed that splashing can be completely suppressed by decreasing the pressure of the surrounding gas. Therefore, we cannot determine the flow field development after liquid droplet impact by utilizing only these three nondimensional numbers, especially when the impact velocities are significant, as in this paper.

It is well known in the field of gas dynamics[31] that another nondimensional number, Ma, which is defined as

$$\mathrm{Ma} = U_i/a_0, \qquad [9]$$

where a_0 is the speed of sound in the gas, plays a significant role in gas flows. It can be easily shown that both the velocity and pressure fields of the gas strongly depend on Ma; hence, a gas flow of significant velocity can be observed even in the cleaning process used for semiconductor production, since a_0, which in general is assumed to be only a function of temperature, and U_i in the present study are of approximately the same order as those used in the cleaning process. Thus, Re, We, and Oh can play only a secondary, not primary, role in high velocity gas flow development.

We observed the high-velocity gas flow field in the strictly limited area in the immediate vicinity of the contact line, as shown in Figure 11ii. An abrupt change in the velocity magnitude distribution in a compressible gas flow is, in general, accompanied by a substantial pressure;[31] hence, we recognize that a considerable pressure can develop after the impact of a droplet at a high velocity. We now discuss the numerical analysis of this possibility. Figure 14 shows the pressure distributions corresponding to those of the r-direction gas velocity magnitude that are presented in Figure 11. The gas pressure is of the order of 1.2 MPa at $t = 10.21$ μs in the vicinity of $r = 0.18\ r_D$. This considerable pressure leads to shock wave propagation. We propose that this pressure, together with its associated shock waves, can contribute to the cleaning process used in semiconductor production.

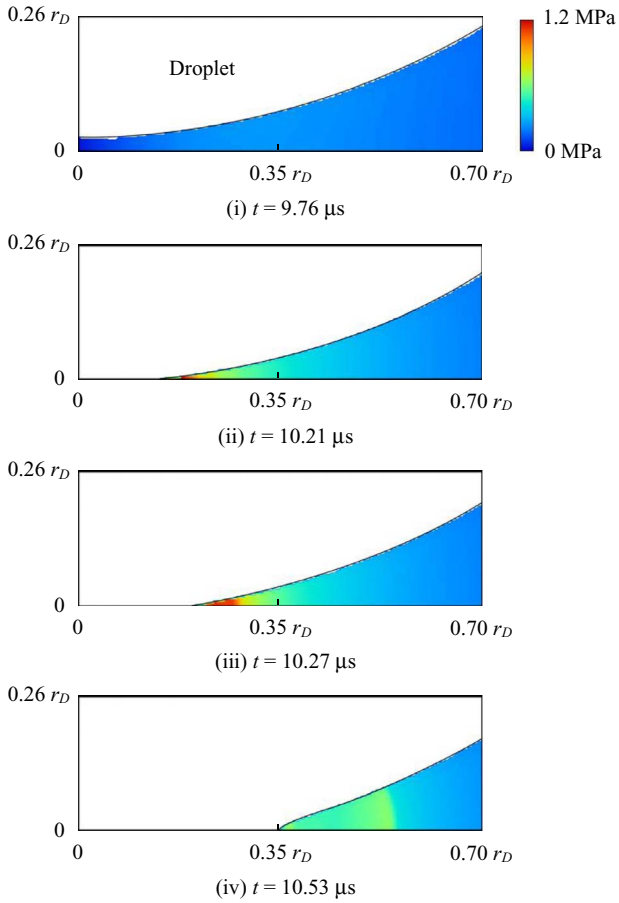

Figure 14. Numerically calculated gas pressure distributions in area shown in Figure 12. Gas pressure is of the order of 1.2 MPa at $t = 10.21$ μs in the vicinity of $r = 0.18\ r_D$.

The LSC method is widely known as an effective means of eliminating particulates from solid surfaces.[6,32–34] Lim et al.[6] measured the cleaning performance of the LSC method by using micron-sized alumina particles attached to a silicon surface. They confirmed that the removal of particles in the LSC process strongly correlates with the dynamics of the laser-induced breakdown (LIB)[32]-generated shock waves of the order of 1.0 MPa. They also showed that the cleaned area increases almost linearly with the intensity of the laser-generated shock. Furthermore, they clearly explained how the cleaning force acts on a particle first because of the net pressure difference when the shock passes over the particle and then because of the dynamic pressure associated with the high-speed gas flow behind the shock front.

We should recall that shock waves of the order of 1.2 MPa, which is about the same as the order of those measured by Liu et al., can develop in gases after droplet impacts at velocities of the order of 50 m/s; hence, we expect that shock waves caused by droplet impacts can also effectively eliminating particulates from solid surfaces.

Conclusions

Both experimental and numerical analyses were used to investigate water-droplet impacts with velocities of up to 50 m/s and the subsequent flow fields, focusing particularly upon the gas flow field. First, the velocity of the splash, which was considered to be a gas–liquid two-phase mist flow, was experimentally evaluated by processing images taken by high-speed photography at rates of up to one million frames per second. The r-direction velocity of the splash, U_s, was approximately 500 m/s when the droplet impact velocity was $U_{ip} = 50$ m/s. The splash could be accelerated by the surrounding gas; hence, the maximum gas velocity was on approximately the same order as U_s. These experimental results led us to conclude that a gas flow field with a high velocity can develop after droplet impact.

The maximum value, U_g, of the r-directional gas velocity was numerically evaluated by solving the Euler equation for a two-phase compressible fluid. Comparison of the velocities, U_s and U_g, supported our conclusion that the maximum gas velocity may be on approximately the same order as U_s; hence, we conclude that a gas velocity field of the order of 500 m/s indeed developed after the impact of droplets with velocities of the order of 50 m/s.

We observed the high-velocity gas flow field in the strictly limited area in the immediate vicinity of the contact line. An abrupt change in the velocity magnitude distribution of a compressible gas flow is, in general, accompanied by a substantial pressure; hence, we recognized that considerable pressure could develop after a high-velocity droplet impact. This possibility was explored via numerical analysis, and the gas pressure was found to be of the order of 1.0 MPa. This substantial pressure led to shock wave propagation. Therefore, we propose that the shock wave propagation in the subsequent gas flow field can contribute to the cleaning process used in semiconductor production in a similar manner to that of the laser shock cleaning method.

Acknowledgments

The authors would like to show their gratitude to Professor Emeritus Shigeo Fujikawa of Hokkaido University for most important advice and to Yasutaka Sakurai and Keiya Sato for their devoted efforts in performing the experiments. This work was supported in part by a Grant-in-Aid for Scientific Research (B) (22360073, 26289031) from JSPS.

References

1. T. Hattori, *ECS Trans.*, **25**(5), 3 (2009).
2. I. Kanno, N. Yokoi, and K. Sato, *ECS Proc.*, **97-35**, 54 (1998).
3. T. Sanada, M. Watanabe, M. Shirota, M. Yamase, and T. Saito, *Fluid Dyn. Res.*, **40**, 627 (2008).
4. T. Sanada, M. Watanabe, A. Hayashida, and Y. Isago, *Solid State Phenom.*, **146**, 273 (2009).
5. T. G. Kim, K. Wostyn, P. Mertens, A. A. Busnaina, and J. G. Park, *ECS Trans.*, **11**(2), 123 (2007).
6. H. Lim, D. Jang, D. Kim, and J. W. Lee, *J. Appl. Phys.*, **97**, 054903 (2005).
7. M. Sato, K. Sotoku, K. Yamaguchi, T. Tanaka, M. Kobayashi, and S. Nadahara, *ECS Trans.*, **41**(5), 75 (2011).
8. Y. Hsueh, C. Chien, M. Yeh, S. Ku, C. M. Yang, C. C. Chen, S. M. Jang, K. Izumoto, K. Sotoku, T. Tanaka, M. Sato, H. Shirakawa, and M. Tanaka, *Solid State Phenom.*, **195**, 195 (2013).
9. H. F. Okorn-Schmnidt, F. Holsteyns, A. Lippert, D. Mui, M. Kawaguchi, C. Lechner, P. F. Frommhold, Ti. Nowak, F. Reuter, M. B. Pique, C. Cairos, and R. Mettin, *ECS J. Solid State Sci. Technol.*, **3**(1), N3069 (2014).
10. M. M. Driscoll and S. R. Nagel, *Phys. Rev. Lett.*, **107**, 154502 (2011).
11. A. Mongruel, V. Daru, F. Feuillebois, and S. Tabakova, *Phys. Fluids*, **21**, 032101 (2009).
12. N. Z. Mehdizadeh, S. Chandra, and J. Mostaghimi, *J. Fluid Mech.*, **510**, 353 (2004).
13. K-L. Pan, K-C. Tseng, and C-H. Wang, *Exp. Fluids*, **48**, 143 (2010).
14. C. W. Visser, P. E. Frommhold, S. Wildeman, R. Mettin, D. Lohse, and C. Sun, *Soft Matter*, (2014).
15. L. Xu, W. W. Zhang, and S. R. Nagel, *Phys. Rev. Lett.*, **94**, 184505 (2005).
16. J. Liu, H. Vu, S. S. Yoon, R. Jepsen, and G. Aguilar, *Atomization and Sprays*, **20**, 297 (2010).
17. B. H. Bang, S. S. Yoon, H. Y. Kim, S. D. Heister, H. Park, and S. C. James, *Int. J. Multiphase flow*, **37**, 55 (2011).
18. K. K. Haller, Y. Ventikos, and D. Poulikakos, *J. Appl. Phys.*, **92**(5), 2821 (2002).
19. A. Harten, B. Engquist, S. Osher, and S. R. Chakravarthy, *J. Comput. Phys.*, **71**, 231 (1987).
20. C.-W. Shu and S. Osher, *J. Comput. Phys.*, **83**, 32 (1989).
21. D. Enright, R. Fedkiw, J. Ferziger, and I. Mitchell, *J. Comput. Phys.*, **183** (2002).
22. R. Saurel and R. Abgrall, *SIAM J. Sci. Comput.*, **21**, 1115 (1999).
23. M. Sussman, P. Smereka, and S. Osher, *J. Comput. Phys.*, **114**, 146 (1994).
24. G.-S. Jiang and D. Peng, *SIAM J. Sci. Comput.*, **21**, 2126 (2000).
25. R. P. Fedkiw, T. Aslam, B. Merriman, and S. Osher, *J. Comput. Phys.*, **152**, 457 (1999).
26. K. Kobayashi, Y. Jinbo, and H. Takahira, *Trans. JSME*, **B77** (2011).
27. C. Mundo, M. Sommerfeld, and C. Tropea, *Int. J. Multi. Flow*, **21**, 151 (1995).
28. P. Walzel, *Chem. Ing. Tech*, **52**, 338 (1980).

29. G.E. Cossali, A. Coghe, and M. Marengo, *Exp. Fluids*, **22**, 463 (1997).
30. R.I. Vender Wal, G.M. Berger, and S.D. Mozes, *Exp. Fluids*, **40**, 23 (2006).
31. H. W. Liepmann and A. Roshko, *Element of Gas Dynamics*, John Wiley & Sons, New York (1957).
32. H. Lim and D. Kim, *Appl. phys. A*, **79**, 965 (2004).
33. M. D. Murthy Peri, V. K. Devarapalli, and C. Cetinkaya, *J. Adhesion Sci. Technol.*, **21**, 331 (2007).
34. T. J. Dunbar and C. Cetinkaya, *Appl. Phys. Lett.*, **91**, 051912 (2007).